

MSC-05546

NASA CR-

141752

(NASA-CR-141752) SKYLAB PROGRAM: EARTH
RESOURCES EXPERIMENT PACKAGE. SENSOR
PERFORMANCE EVALUATION. VOLUME 6: (S194)
L-BAND RADIOMETER Final Report (Martin
Marietta Corp.) : 57 p HC \$4.25

N75-21589

Unclas
18638

CSSL 476 G3/35

SKYLAB PROGRAM

EARTH RESOURCES EXPERIMENT PACKAGE

SENSOR PERFORMANCE EVALUATION
FINAL REPORT
VOLUME VI (S194)



APRIL 7, 1975

CONTRACT NAS8-24000

AMENDMENT JSC-14S



National Aeronautics and Space Administration
LYNDON B. JOHNSON SPACE CENTER
Houston, Texas

MSC-05546

EARTH RESOURCES EXPERIMENT PACKAGE

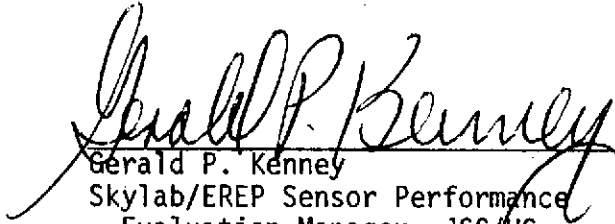
SENSOR PERFORMANCE REPORT

VOL. VI (S194)

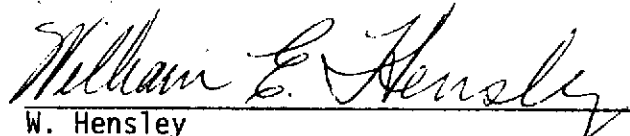
FINAL REPORT

April 7, 1975

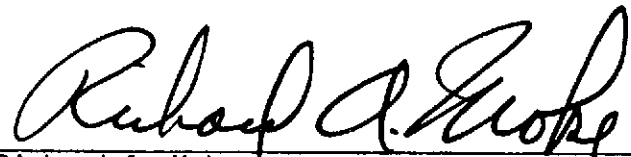
Submitted by:


Gerald P. Kenney
Skylab/EREP Sensor Performance
Evaluation Manager, JSC/HC

Technical
Review by:


W. Hensley
S194 Project Scientist, JSC/TF

Approved:


Richard A. Moke
Manager, Systems Analysis and
Integration Office, JSC/HC

Contract NAS8-24000
Amendment JSC-14S

Skylab Program
Lyndon B. Johnson Space Center

FOREWORD

This document is Section VI of six sections of document MSC-05546, titled "Earth Resources Experiment Package, S194 Sensor Performance Evaluation." This document is the final report on the sensor performance evaluation results and includes recommendations for future programs for the evaluation of microwave sensors.

CONTENTS

	<u>Page</u>
Acknowledgment	VI-i
Foreword	VI-ii
Contents	VI-iii
1. INTRODUCTION	VI-1
1.1 Purpose	VI-1
1.2 Scope	VI-1
1.3 Usage Guide	VI-1
1.4 Abstract	VI-2
2. APPLICABLE DOCUMENTS	VI-2
3. SUMMARY OF SENSOR PERFORMANCE EVALUATION	
INTERIM REPORT	VI-3
3.1 Function/Limit Verification (SPE-S194-001)	VI-3
3.1.1 Housekeeping Data Engineering Limit Verification	VI-3
3.1.2 Internal Calibration Data Analysis	VI-4
3.1.3 Engineering Limit Violations	VI-6
3.1.4 Control and Display Panel Status/ Malfunction Indicator Anomalies	VI-6
3.1.5 Preflight Analysis of Radiometric Temperature Data	VI-7
3.1.6 Antenna Pointing Check	VI-7
3.2 Interference Check (SPE-S194-002)	VI-7
3.2.1 S194 Preflight EMI Compatibility Tests	VI-8
3.2.2 S194 EMI Compatibility during Skylab Missions SL2, SL3, and SL4	VI-8
3.2.3 Contamination Effects Evaluation	VI-9
3.3 Brightness-Temperature Precision/Accuracy (SPE-S194-003)	VI-9
3.3.1 Simulation Models	VI-9
3.3.2 Evaluation of Precision and Accuracy Using Flight Data	VI-10
3.4 Radiometer Receiver Dynamic Range/Linearity/ Sensitivity (SPE-S194-004)	VI-16
3.4.1 Dynamic Range	VI-16
3.4.2 Sensitivity	VI-16
3.4.3 Linearity	VI-17
3.5 Antenna Performance and Resolution (SPE-S194-005)	VI-18
3.5.1 Antenna Performance	VI-18
3.5.2 Antenna Resolution	VI-18

	<u>Page</u>
3.6	Baseline and Gain Stability (SPE-S194-006) VI-18
3.6.1	Radiometer Stability over Homogeneous Targets VI-19
3.6.2	Sun-Angle Error Estimates VI-19
3.6.3	Radiometer System Time Response VI-21
3.7	Radiometer Combined Insertion Loss (SPE-S194-007) VI-21
3.7.1	Qualification of Deep-Space Brightness. VI-21
3.7.2	System Calibration from SL2 Deep-Space Data VI-21
3.7.3	Insertion Loss Evaluation VI-22
3.7.4	Thermal Effects on Insertion Loss VI-23
4.	FINAL RESULTS VI-25
5.	CONCLUSIONS VI-28
5.1	Housekeeping and Internal Calibration Data VI-28
5.2	Radiometric Data VI-28
5.3	Antenna Integrity VI-29
6.	RECOMMENDATIONS VI-30
7.	NOTES VI-32
7.1	Acknowledgments VI-32
7.2	Abbreviations VI-32

Appendix A

I. Evaluation of S194 Radiometric Temperature Error Due to Pointing Uncertainties	A-1
A. Sensor Installation and Skylab Attitude Uncertainties	A-1
B. Estimate of Radiometric Temperature Error Due to Pointing Uncertainties	A-2
II. Skylab S194 Radiometer Calibration	A-5
A. Relationship between T_{AC} , T_{SA} , and T_{PA}	A-6
B. Calibration - The Balance Equations	A-9
C. Effect of Cold-Load Temperature on T_e	A-15

1. INTRODUCTION

1.1 Purpose

This document reports the final results of the sensor performance evaluation of the Skylab Earth Resources Experiment Package (EREP) S194 L-Band Radiometer, and is based on data and evaluations reported in the interim performance evaluation report (MSC-05528, Volume VI, dated September 6, 1974).

1.2 Scope

This document summarizes the results of the S194 L-band radiometer sensor performance evaluation based on data presented by all contributors (Lockheed Electronics Company, Science and Applications Directorate, NASA Johnson Space Center and Martin Marietta Corporation) to the sensor performance evaluation interim reports, provides the results of additional analyses of S194 performance, and describes techniques used in sensor performance evaluation (Appendix A). The summarization includes S194 and EREP system anomalies that affected S194 performance, and the performance achieved, in terms of pertinent S194 parameters. The additional analyses include final performance analyses completed after submittal of the S194 interim sensor performance evaluation reports, including completion of detailed analyses of basic performance parameters initiated during the interim report periods.

1.3 Usage Guide

The basic task outline for the EREP sensor performance evaluation was specified in EREP Mission Data Evaluation Requirements, JSC-05529, August 31, 1973. The results of these evaluations were subsequently reported in MSC-05528, Earth Resources Experiment Package, Sensor Performance Report, Volumes I through VII, as follows:

Volume I (S190A)	Multispectral Photographic Camera
Volume II (S191)	IR Spectrometer
Volume III (S192)	Multispectral Scanner
Volume IV (S193 R/S)	Radiometer/Scatterometer
Volume V (S193 Alt.)	Altimeter
Volume VI (S194)	L-Band Radiometer
Volume VII (S190B)	Earth Terrain Camera

These volumes were issued after prelaunch testing at KSC and updated after each mission. The single exception is Volume VII (SL90B), which was originally issued after SL3, with a single update after SL4.

This document is based on the data and analyses in the first six volumes of the Sensor Performance Report, MSC-05528 (Volume VII, SL90B, is not included). The same volume designation used for MSC-05528 has been retained for the individual sensor volumes, with the individual volumes bound in a single cover and identified as MSC-05528. The individual volumes are designed so they can be used independently of the full six-volume report, if desired.

1.4 Abstract

Analysis of the Skylab SL94 L-Band Radiometer experiment data has provided many significant results pertaining to the actual realized performance during flight. Analysis of preflight test data has provided a baseline from which to compare the experiment flight performance, although many radiometric data performance capabilities could only be demonstrated in the flight environment. The final results establish the overall hardware performance of the SL94 system from which prospective users of the flight data can refer for various scientific applications.

Agencies participating in the SL94 sensor performance evaluation were the Science and Applications Directorate of Lyndon B. Johnson Space Center, Lockheed Electronics Company Aerospace Systems Division, and the Denver Division of Martin Marietta Corporation. Instrument performance is presented in the areas of housekeeping and internal calibration parameters, antenna system integrity, dynamic range, linearity, precision, resolution, and absolute accuracy. Supplementary evaluations have been included for an error analysis of system calibration stability. Results of the evaluation show that the instrument performance was generally as expected.

Conclusions are drawn from the final evaluation results, and recommendations for improving the effectiveness of a future program are offered.

2. APPLICABLE DOCUMENTS

MSC-05528	<u>Earth Resources Experiment Package, Sensor Performance Report, Volume VI (SL94), Engineering Baseline, SL2, SL3, and SL4 Evaluation</u> , Lyndon B. Johnson Space Center Houston, Texas, September 6, 1974.
PHO-TR 524	<u>Earth Resources Production Processing Requirements for EREP Electronics Sensors</u> , Lyndon B. Johnson Space Center, Houston, Texas, January 3, 1974.

3. SUMMARY OF SENSOR PERFORMANCE EVALUATION INTERIM REPORT

This section summarizes the S194 hardware performance data documented in the Baseline/SL2/SL3/SL4 Sensor Performance Evaluation (SPE) Interim Report, MSC-05528, Volume VI, dated September 6, 1974. The summary provides a description of each sensor performance evaluation task, including scope, approach used, and important findings derived from these analyses. References will be made to the cumulative body of performance data in MSC-05528 to provide additional detail and supporting data for the results summarized.

3.1 Function/Limit Verification (SPE-S194-001)

The general health and integrity of the S194 radiometer system was established by a review of housekeeping data, internal calibration data, and control and display panel status and malfunction indicator responses. Criteria for acceptable operating limits were established for each of the 13 housekeeping parameters and for internal calibration. These criteria reflect normal expected limits based on design goals and operational environment.

3.1.1 Housekeeping Data Engineering Limit Verification

Details of the housekeeping data analysis from KSC tests, missions SL2, SL3, and SL4, are in Section 3.1 of MSC-05528, Volume VI. Principal results of these analyses are summarized in the following paragraphs.

3.1.1.1 Preflight Results - Due to the terrestrial test environment, meaningful data were only obtained for the hot-source reference-noise generator (RNG) temperature and for power-supply voltage monitors. During all preflight tests, the hot RNG remained at a stable temperature of 372.84°K . The voltage monitors indicated excellent regulation for the power supply, with no change in value for the +5- and -5-volt supplies, and only periodic 4-bit step changes (the minimum digital resolution for the +12- and -12-volt supplies. Data obtained for the five antenna monitors, enclosure monitor, and two cold-load

RNGs essentially showed that these monitors were functional. However, the test environment prevented these systems from operation in their normal ranges.

3.1.1.2 In-flight Results - Most housekeeping data obtained during flight provided values within expected ranges. Specifically, the five antenna-temperature monitors and four power-supply voltage monitors performed as expected, indicating satisfactory performance throughout all Skylab missions. However, there were some unexpected results. On all Skylab passes, the two cold-load RNGs operated at higher temperatures than expected. For most passes, at least one of the two cold-load RNGs remained within the operating range of their thermal monitors, and thus a valid calibration was still possible. On a few passes, both cold loads exceeded their upper temperature limits, and normal data-reduction programs could not be used. Special software programs were developed to permit processing data like these, using valid calibration data from other passes. To date, no data reprocessed in this manner have been reviewed. Therefore, the accuracy of data obtained using this technique has not been verified.

During SL2, the inability of the electronics box enclosure heater to achieve and maintain its design temperature (approximately 297°K) directly affected hot calibration-source and hot reference-source warm-up times. For several passes in SL2, the planned 30-minute warm-up was insufficient to permit the hot calibration source and hot reference source to reach design temperatures before the start of the data pass, resulting in invalid calibration for these passes. Special thermal tests conducted by the SL94 hardware contractor (AIL Division of Cutler Hammer) provided correction equations to compensate for insufficient hot RNG warm-up, and for changing enclosure temperatures. The detailed derivation of these correction equations is in Section 3.2.2.3 and Appendix A of MSC-05528, Volume VI. The problem of low temperature for the hot RNG was rectified on SL3 and SL4 by increasing the prepass warm-up times. However, the low enclosure temperature was present throughout all Skylab missions.

3.1.2 Internal Calibration Data Analysis

Analysis of calibration data from KSC tests and from Skylab flight was used to verify the stability of hot calibration-source data as well as to establish the functional performance of the calibration logic. The details of the calibration data analysis are in Section 3.2 of MSC-05528, Volume VI, and primary results are summarized in the following paragraphs.

3.1.2.1 Preflight Results - Operation of the calibration logic, i.e., mode sequencing scheme duration of operation in each calibration submode, and intervals between automatically initiated calibration sequences, was established in the many preflight tests. Operation of the calibration logic was shown to be repeatable for all calibration sequences, meeting all criteria established. Stabilization of radiometric data in each submode was seen to be rapid enough to provide reliable values for calibration data.

An evaluation of the radiometer's ability to meet the design requirements of its end item specification (EIS) for absolute accuracy and precision was made insofar as possible from KSC test data, using the internal hot calibration source as a "known" input noise temperature. This evaluation was necessarily limited to the performance of radiometer electronics, exclusive of the antenna, because calibrated inputs to the antenna were not available. Some inaccuracies may have been introduced in this analysis due to the use of an empirically derived equation and the use of some individual loss terms that are normally combined in overall system measurements. However, the results of this analysis did provide good indications that the radiometer absolute accuracy of $\pm 1^{\circ}\text{K}$ and precision (RMS deviation) of $\pm 0.5^{\circ}\text{K}$ could be met at this level of input noise temperature.

3.1.2.2 In-flight Results - Operation of the calibration logic during flight was identical to that seen in the KSC test data. No malfunctions or changes in operation were observed in any Skylab in-flight calibration data. Except for those few passes during SL2 when the hot load had not reached stable-operation temperature, the hot-calibration radiometric data showed excellent stability, ($< 0.5^{\circ}\text{K}$ variation) and was repeatable from pass to pass, mission to mission.

The mean and standard deviation of the hot calibration-source radiometric data, referenced to the radiometer input terminal, is shown in Table 3.1.2.2-1 for representative samples of each Skylab mission. For comparison, the statistics for hot calibration data from KSC tests are also shown. Because of the large amount of data produced during test and flight, these statistics were based on only a portion of the total data available. However, the data evaluated represent a reasonably large sample base, and were derived from sample data covering the total spectrum of different environmental situations.

Because the cold-calibration radiometric data fluctuates over a broad range from pass to pass, due to differing thermal conditions, evaluation of cold calibration data was limited to verification of data stability for each individual calibration sequence and verification that cold loads were operating within the range of their thermal monitors. The stability of cold calibration radiometric data for individual calibration sequences was shown to be very good; comparable to the hot calibration data. However, on several passes, the cold calibration temperatures exceeded the operational range of their thermal monitors, resulting in invalid calibration for these passes. The passes affected by invalid calibrations are itemized in Section 3.1.3 of MSC-05548, Volume VI.

Table 3.1.2.2-1 Statistics for Hot Calibration Data

TEST/MISSION PERIOD	HOT CALIBRATION-SOURCE RADIOMETRIC TEMPERATURE ($^{\circ}$ K) (Referenced to Radiometer Input Terminal)	
	Mean	Standard Deviation
KSC	370.3	0.415
SL2	370.2	0.133
SL3	371.0	0.154
SL4	371.0	0.195

3.1.3 Engineering Limit Violations

Section 3.3 of MSC-05528, Volume VI, provides an itemized tabulation of housekeeping and internal calibration data anomalies that occurred during the three Skylab missions. No anomalies were observed for KSC tests. For this analysis, an anomaly was identified as any occurrence of a data value outside expected operating limits. Criteria for expected operating limits were established before flight. In many cases, indication of an anomaly did not necessarily imply that the radiometric data was degraded. The tables in Section 3.3 of MSC-05528, Volume VI, identify the pass number, a description of the anomaly and the data affected by each housekeeping or calibration data anomaly uncovered in the data evaluation. Obvious computer-generated "wild points" were not treated as anomalies. Those anomalies that were considered to have affected the radiometric data were included in the in-flight recalibration evaluation and are not further covered here.

3.1.4 Control and Display Panel Status/Malfunction Indicator Anomalies

Status/malfunction lamps on the EREP control and display panel applicable to SL94 sensor operation were observed during all test and flight periods because their proper operation provided additional insight into the general condition of the instrument. Crew comments in real time, from the postpass debriefings, and in the postpass summary reports, were used as the primary source of data for evaluating control and display panel indicator status. A review of the procedures, timelines, and housekeeping data was also made to verify that criteria for satisfying indicator logic circuits had not been violated. The only abnormal lamp operation reported was the result of transient response conditions not previously identified. It was verified

that these conditions had no effect on normal sensor operation or data quality. The details of the analysis of status/malfunction indicator anomalies is in Section 3.4, MSC-05528, Volume VI, along with a description of operational criteria for each S194 indicator.

3.1.5 Preflight Analysis of Radiometric Temperature Data

Evaluation of antenna radiometric brightness-temperature data during KSC tests was severely limited because of the presence of the antenna cover during all tests. There were no sources of calibrated input to the antenna. The measured antenna brightness was expected to be approximately that of the ambient room temperature and to remain reasonably stable. Because the influence of the antenna cover on the antenna near-field pattern was unknown, the criteria for acceptable operation were necessarily quite broad. A diode noise source and dipole element mounted on the antenna cover were operated to verify the continuity of the antenna to the radiometer electronics. The noise source was adjusted to provide an effective net increase in measured brightness of approximately 30°K. Results of the antenna brightness data evaluation during KSC tests indicated that all test criteria for data mean values as well as data stability were met. Section 3.5 of MSC-05528, Volume VI, reports the details of this analysis.

3.1.6 Antenna Pointing Check

As part of the sensor performance evaluation, an analysis has been performed to determine the uncertainty in the SKYBET determination of S194 sensor antenna boresight pointing direction with respect to the local vertical. This analysis was based primarily on the analytical study performed by the Mathematical Physics Branch of the Mission Planning and Analysis Division at JSC. Based on the computed uncertainty in attitude pointing, an evaluation was made to determine the magnitude of antenna brightness-temperature error that might be expected from the S194 radiometer. This analysis showed that, for pointing errors of the magnitude indicated, the potential worst-case error in S194 radiometric measurements was small enough to be ignored. A detailed description of the techniques used to establish the magnitude of pointing uncertainty and to derive the effects of pointing error on radiometric measurement accuracy are in Section 3.6 of MSC-00528, Volume VI, and Appendix A, Section I, of this volume.

3.2 Interference Check (SPE-S194-002)

This section summarizes the assessment of electrical (EMI) and contamination interference effects on radiometer operation.

3.2.1 S194 Preflight EMI Compatibility Tests

Analysis of S194 EMI compatibility with other Skylab systems was severely limited during preflight tests due to the use of a cover on the S194 antenna face as protection against possible damage to the receiver from an unknown EMI environment during the test as well as for physical protection. The protective cover essentially prevented any meaningful total system tests of the susceptibility of the S194 to radiated EMI.

A special EMI test was performed with the S194 and the inverter lighting control assemble (ILCA), which was on the same mounting structure behind the S194 antenna. This special test was conducted because of the close proximity of the ILCA to the S194, and the decision to waive EMI qualification testing of the ILCA. Results of this test indicated that the ILCA did not interfere with the S194.

Another special bench test was performed to evaluate the susceptibility of S194 to interference from the S193 radar. To limit the amount of energy coupled to S194, special low-pass filters were added to S194 that could reduce the K_u -band contributions to a negligible value. This was verified in special bench tests on the electronics without the antenna.

Possible effects of conducted EMI were evaluated as a normal part of every preflight system-test data review. The primary parameter investigated for determination of EMI effects was the radiometric data output. Because all S194 data were essentially constant throughout each test, any change in value would be readily apparent in the data review. No effects of conducted EMI were evident in data obtained from preflight test. Further details on EMI evaluations for scheduled preflight tests, as well as results of special tests set up for EMI investigations, are in Section 4.1.1 of MSC-05528, Volume VI.

3.2.2 S194 EMI Compatibility During Skylab Missions SL2, SL3, and SL4

S194 data for all EREP passes were reviewed to assess EMI compatibility during flight. Tabulations and strip charts of S194 housekeeping and scientific data were reviewed for any sudden or unexplained changes in value that might be attributed to EMI. The review showed occasional sporadic response in the science data, which is believed to be attributable to interference from ground-based radars. The total number of EMI incidents for all Skylab missions is small, perhaps 10 to 15 in all, with the majority of these occurring for only one to three sample periods (typically between 1/3 and 1 second in duration). Four especially interesting EMI incidents, one during SL3, and three during SL4, were observed. They consisted of very erratic responses from the S194 for 20 seconds or more. These occurred on DOYs 223, 334, 348, and 027, and are all similar. It is believed that these EMI disturbances seen in the S194 data were caused by reflected energy from commercial air route traffic control radars or military air traffic control systems. A review of crew procedures and Skylab hardware status during each suspected S194

EMI incident showed no correlation between the EMI occurrences and any Skylab activity.

The EMI incidents were easily identified in the data and these data could be discarded, as appropriate. The total amount of data lost or made unusable as a result of EMI is insignificant. A detailed analysis of EMI investigations affecting S194 flight data is in Sections 4.1.2, 4.1.3, and 4.1.4 of MSC-05528, Volume VI, dated September 6, 1974, for Skylab missions SL2, SL3, and SL4, respectively.

3.2.3 Contamination Effects Evaluation

There was no contamination assessment during preflight testing because all test activities were conducted in a clean room. Contamination evaluation during flight considered the effects of short-term or specific contamination events as well as long-term cumulative effects. Possible contamination effects on three critical S194 surfaces, i.e., antenna face, cold-load horn internal surfaces, and electronics-box thermal-control surface, were examined after each Skylab mission. The analysis included a review of selected S194 data parameters such as antenna brightness and component thermal temperatures, as well as comparison of contamination deposition levels as predicted by a computer contamination model with susceptibility threshold levels that had been established for S194 surfaces.

Although computed deposition levels on cold load horns and the electronics-box thermal-control surface exceeded established susceptibility threshold levels during the SL4 mission, analyses of the S194 data indicated no effects on any S194 measurement parameter, and no apparent degradation of experiment operation throughout all Skylab missions. The development of susceptibility criteria and evaluation techniques for contamination effects evaluation are in Section 4.2 of MSC-05528, Volume VI, dated September 6, 1974. Assessment of contamination effects for each Skylab mission is in Sections 4.2.1, 4.2.2, and 4.2.3 of MSC-05528 for SL2, SL3, and SL4, respectively.

3.3 Brightness-Temperature Precision/Accuracy (SPE-S194-003)

This section summarizes the evaluation of brightness-temperature precision and accuracy.

3.3.1 Simulation Models

As a baseline from which to compare and evaluate the quality of antenna brightness temperature data, mathematical models were developed for the sensor and for sea-surface target brightness simulation. The sensor mathematical model developed the system equations used to express any input radiometric

brightness temperature in terms of the measured output Y-factor, known or measured loss factors, and component thermal temperatures. The equations developed are those used in the production data processing (PDP) of the S194 flight data and presented both in the interim sensor performance evaluation reports and the production data processing documentation.* There was also a sea-surface simulation model for calculating sea-surface brightness temperatures, assuming a calm sea and no cloud cover. This was based on a computer model developed by Dr. J. Paris of Lockheed Electronics Co. To predict sea-surface brightness temperatures referenced to Skylab altitude, corrections to the model were developed for atmospheric contributions and antenna pattern effects.

An error analysis of the sensor mathematical model was conducted to define boundaries of expected uncertainties for S194 antenna measurements. The output of the error model was a curve that presented the three-sigma (3 σ) cumulative uncertainties in measured antenna brightness as a function of input antenna brightness. A detailed presentation of the development of these models is in Sections 5.1.1, 5.1.2, and 5.1.2 of MSC-05528, Volume VI, dated September 6, 1974.

3.3.2 Evaluation of Precision and Accuracy Using Flight Data

Large homogeneous target areas were selected from each Skylab mission for evaluation of S194 precision and absolute accuracy. (See Appendix E, MSC-05528, Volume VI for detailed analysis). Targets for this evaluation included deep space, the Gulf of Mexico, Sahara Desert, Great Salt Lake Desert, and the Ar Rub Al Khali (Great Sandy Desert in southern Arabia). These targets were selected to encompass the largest possible portion of the dynamic range of the sensor as well as for their uniformity over the large field of view of the antenna. Tabulations of meteorological data and lists of applicable S190A photographic frame numbers were provided for each target evaluated. These supporting data were to aid in establishing the atmospheric and target surface conditions during each selected target pass. A summary of the results from the four aircraft program MFMR L-band data flights are also provided for comparison with Skylab S194 L-band data.

3.3.2.1 Brightness-Temperature Absolute Accuracy - All passes from each Skylab mission over the selected target areas were evaluated. Brightness-temperature absolute accuracy for all passes over the Gulf of Mexico were evaluated by comparing the mean value of measured brightness to the sea-target simulation-model predicted range. The predicted range of all passes over the Gulf of Mexico was established to be 93.9°K to 96.7°K, using the

*Earth Resources Production Processing Requirements for EREP Electronic Sensors, PHO-TR524, NASA/JSC, 3 January 1974.

target simulation model with the estimated normal range of expected humidity based on U.S. Standard Atmospheric data, and an expected range of sea-surface temperature of 10°C . The criterion for absolute accuracy of the Gulf data was taken to be the arithmetic sum of the sea-target simulation-model range (93.9 to 96.7°K) plus the 3σ uncertainty error limits established by the error model (approximately $\pm 4.5^{\circ}\text{K}$ at sea brightness temperatures.) With the exception of those passes for which the sun contribution was known to be excessive, or precipitation was known to be present, all data for the Gulf of Mexico fell within the 3σ error limits, thereby verifying the absolute accuracy of the instrument, within the limits of the model. (This analysis also excluded SL4 Pass 53 for which Skylab was in a solar inertial attitude).

The criterion for all deep space passes was established to be 3°K plus the 3σ error model limits (approximately $\pm 7.5^{\circ}\text{K}$ at deep-space brightness temperatures). All deep-space data were well within the 1σ limits ($\pm 2.5^{\circ}\text{K}$). No criteria for absolute accuracy of data over the Great Salt Lake Desert, Sahara Desert, or Rub Al Khali were available because there were no suitable aircraft or ground truth data from which to construct a desert simulation model.

3.3.2.2 Brightness Temperature Relative Accuracy - The relative accuracy evaluation presented in the following paragraphs compares the change in measured antenna brightness temperatures for different target conditions to the change in theoretically predicted brightness temperatures calculated through simulation models. The simulation models in this analysis, which require assuming certain target parameters, are described in Section 9.1.2 of MSC-05528, Volume VI. While it is permissible to assume representative target parameters for simulation models in this relative accuracy comparison, it is not valid to make these assumptions to determine absolute accuracy.

The technique described below demonstrates that the SL94 instrument responded to different input conditions in a predictable manner, verifying the relative accuracy.

3.3.2.2.1 Relative Accuracy for Fresh Water versus Salt Water Targets - Figure 3.3.2.2.1-1 shows plots of measured antenna brightness extending over the Pacific Ocean and over Lake Superior. Over fresh water with an assumed salinity of 0‰ at 16°C , one would expect from the target simulation model that surface brightness, T_{BS} , should be 107.5°K and that antenna brightness, T_{AC} , should be 109.0°K at satellite altitude. This was compared to a nominal observed T_{AC} of 106.5°K over Lake Superior on EREP pass 31, track 16. Because the physical water temperature had a significant effect on measured brightness at low salinities, the water temperature of Lake Superior was obtained from ship data.

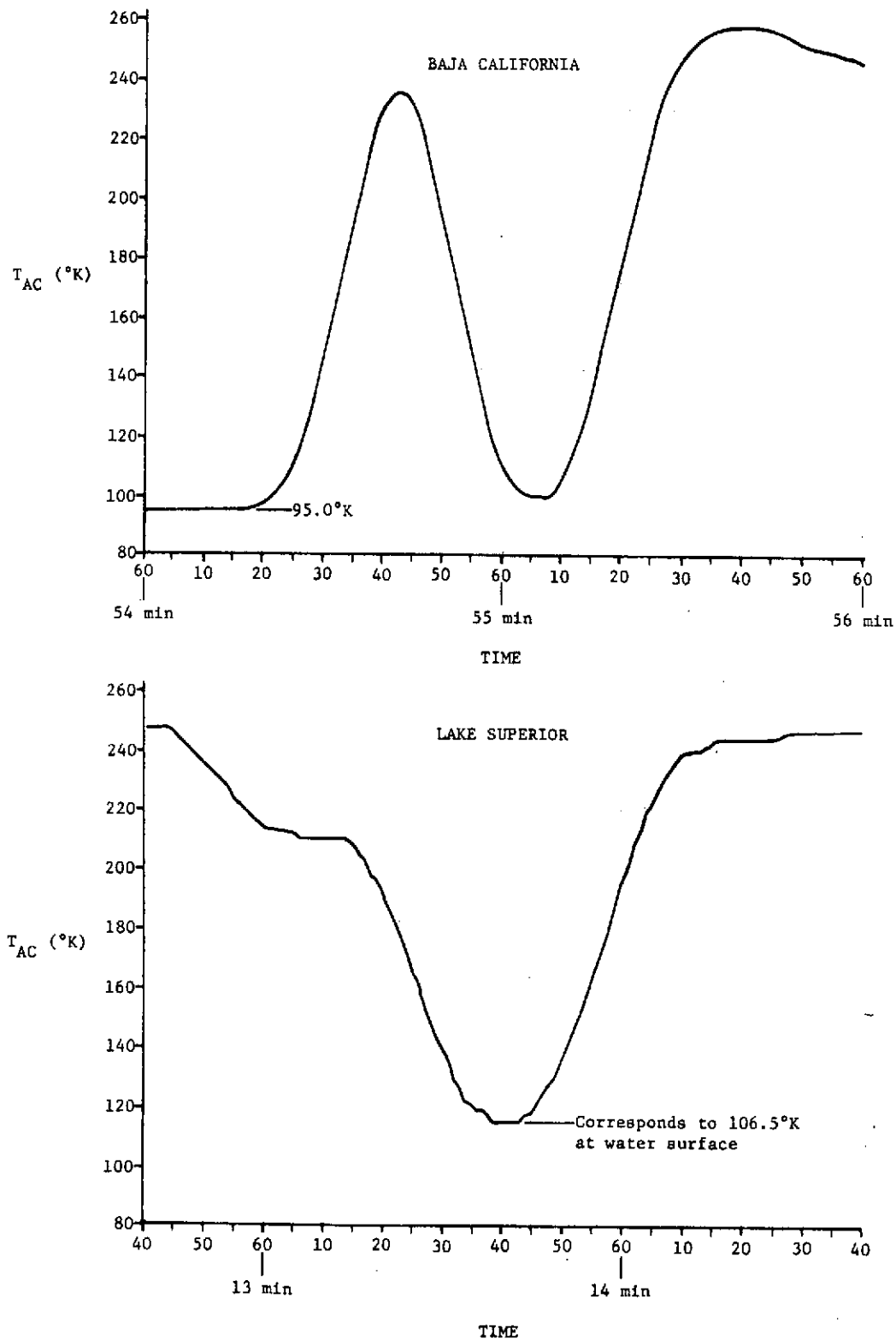


Figure 3.3.2.2.1-1 Fresh-Water and Salt-Water Relative Accuracy

Over sea water with an assumed salinity of 35‰ at 10°C, it was expected from the target simulation model that T_{BS} would be 97.0°K at the surface and T_{AC} would be 98.6°K at satellite altitude. This was compared with a nominal observed T_{AC} of 95.0°K over the Pacific Ocean on EREP pass 38, track 58.

The expected difference in brightness of 10.4°K between fresh and sea water is in good agreement with the nominal measured difference of 11.5°K. A more precise comparison could not be made without appropriate ground truth data. In determining measured brightness for Lake Superior, the surface brightness was derived by convolving the antenna pattern with a brightness model of the ground terrain and fitting the results to the actual measured data. This was required for the Lake Superior site because the antenna pattern was larger than the surface area presented by the boundaries of Lake Superior.

3.3.2.2.2 Relative Accuracy as a Function of Different Surface Temperatures - The relative accuracy of the SL94 radiometer for different surface temperatures is shown by comparing the measured response on two different passes over the Sahara Desert. The first pass occurred on a hot day and the second on a day after a cold front had moved through. Figure 3.3.2.2.2-1 shows that the difference in mean value of measured brightness for these two passes was 17.6°K. From meteorological data provided by NOAA, the atmospheric temperature, t_{atm} for pass 21 was given as 107°F, and for pass 92, as 71°F. Using the atmospheric temperatures provided, and an assumed dielectric constant (ϵ) of approximately 3.2 for the Sahara Desert site, the target simulation model predicted brightness values for passes 21 and 92 were approximately 300.3 and 283.6°K, respectively. The measured difference in mean brightness of 17.6°K compared very favorably with the desert simulation-model predicted difference of 16.7°K.

3.3.2.3 Brightness Temperature Precision - For this sensor performance evaluation task, the term "precision" was defined to be the repeatability of the mean value of measured antenna brightness for passes over the same target area. Evaluation of precision was made without regard to the bias between the true value and measured value of antenna brightness. Results of the precision evaluation for passes during SL2, SL3, and SL4 are summarized in Table 3.3.2.3-1, which does not include data from passes for which target or atmospheric conditions were known to provide an atypical input temperature. There were also a number of passes for which data were not available, or for which data were known to be in error due to processing problems. This limited the number of data points available for evaluation of precision.

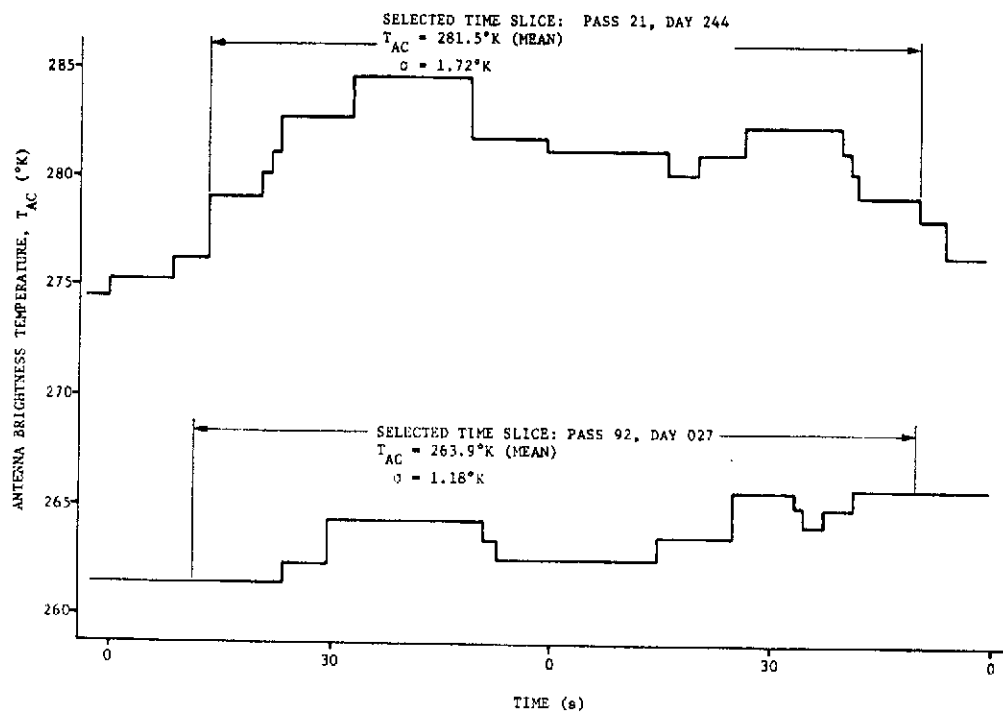


Figure 3.3.2.2.2-1 Hot- and Cold-Surface Thermal-Temperature Relative Accuracy

ORIGINAL PAGE IS
 OF POOR QUALITY

Table 3.3.2.3-1 Repeatability of Antenna Brightness as a Measure of Precision

SKYLAB MISSION	TARGET SITE	NUMBER OF PASSES OVER SITE	REPEATABILITY (Range of Mean Values) (°K)	STANDARD DEVIATIONS (°K)
SL2	Gulf of Mexico	3	3.7	1.9 1.7 2.2
SL3	Gulf of Mexico	4	2.8	1.9 0.7 1.7 2.6
	Great Salt Lake Desert	4	2.9	2.4 1.7 3.0 2.7
	Sahara Desert	2	2.1	1.8 3.2
SL4	Deep Space	2	0.3	0.3 0.3
	Gulf of Mexico	8	5.3	2.0 1.8 2.3 1.7 1.1 1.0 2.0 2.6

3.4 Radiometer Receiver Dynamic Range/Linearity/Sensitivity (SPE-S194-004)

This section summarizes the evaluation of radiometer receiver dynamic range, linearity, and sensitivity.

3.4.1 Dynamic Range

The receiver dynamic range was dictated by the available binary bit-count output and by receiver resolution. However, practically the total dynamic range exercised on Skylab missions was bounded by deep space as the lowest radiometric temperature and the internal hot calibration source as the highest radiometric temperature to be measured. These levels of input radiometric temperature, deep space 23.6°K and internal hot calibration source 372.1°K were measured throughout the Skylab missions. See Appendix E, MSC-05528, Vol. VI for more detailed information on the dynamic range of the radiometer.

3.4.2 Sensitivity

S194 radiometric receiver sensitivity was defined for this sensor performance evaluation task as the instantaneous resolution of the system radiometric data. Sensitivity was monitored by review of the system parameter, K, expressed in degrees Kelvin per bit. The value of K was redefined with each in-flight calibration. A plot of the calculated values for K from selected passes from each Skylab mission was provided in the Appendix E, MSC-05528, Vol. VI to illustrate the variations in sensitivity as a function of time.

It has been shown that there were small variations in sensitivity from pass to pass, and from prepass to postpass. These variations were believed to be predominately a function of different instrument thermal conditions at the time of each in-flight calibration, and to some extent a function of instrument resolution of some housekeeping measurements that were used to calculate K. This evaluation indicated no significant changes or trends in system response throughout the three Skylab missions.

The effects of the change in sensitivity, from a prepass calibration to a postpass calibration, on the variation in the computer value of radiometer input brightness temperature (T_{SA}) was evaluated. This analysis computed the value of T_{SA} for selected data points using the two different values of sensitivity that resulted from the two internal calibration sequences. To determine the variations in T_{SA} due solely to variations in K, calculations for T_{SA} were made holding the values for Y factor (A_A), enclosure temperature (t_D), and RF cable temperature (T_{CA}) constant. However, because the changes

in t_D and t_{CA} tended to compensate for the changes in sensitivity factor, K , the user should not take the K variations so determined as a true indication of the accuracy inherent in the instrument's determination of antenna brightness temperature (T_{AC}). Analyses of sensitivity for selected passes from each Skylab mission were detailed in Appendix E, MSC-05528, Volume VI. The total range of values of K observed in the flight data was approximately 0.82 to 0.86°K per bit.

3.4.3 Linearity

Radiometer receiver linearity was evaluated by tests and examination of flight data.

3.4.3.1 Preflight Linearity Tests - Preflight linearity tests were conducted as part of acceptance testing. (See AIL Specification 00752-375874, Test Data Sheets for S194 Electronics Box Electrical Test/Calibration.) Preflight linearity tests were limited to the electronics box. Thus, no complete system linearity tests were conducted before flight. Receiver linearity was satisfactorily demonstrated to meet the acceptance criterion of less than 2 1/2°K deviation from a best-fit straight line.

3.4.3.2 System Linearity Evaluation from Flight Data - Two different approaches were used to evaluate S194 receiver linearity in the postflight analysis. In the first approach the values of radiometer input brightness temperature, T_{SA} , were plotted as a function of the corresponding values of Y factor for selected data. The selected data were taken from the same targets used for evaluation of brightness temperature precision and accuracy analysis (See Section 3.3.2), which provided brightness temperature values covering a broad portion of receiver dynamic range. Details on this approach and analysis may be found in Appendix E, MSC-05528, Volume VI. The worst case deviation of any data point from the linear least-square fit curve was determined to be approximately 5%.

The second approach to verify radiometer linearity consisted of calculating, through simulation models, predicted brightness temperature values for selected targets and plotting these values versus the measured brightness temperatures. This approach suffers inaccuracies due to the requirement of measured target parameters for input to the simulation models, which for most of the targets is not available. However, the worst case deviation from a linear least-squares fit curve was less than 7% in this case. For details of this approach see Section 6.3 of MSC-05528.

3.5 Antenna Performance and Resolution (SPE-S194-005)

A very detailed digital computer program was developed to simulate target areas of distributed brightness temperatures. Also incorporated into the simulation model were the measured pre-flight antenna gain patterns. Selected target site simulations had not been completed at the writing of this report, however, the complete description of the simulation analysis required to complete this task (SPE-S194-005) is presented in Appendix E, MSC-05528, Volume VI.

3.5.1 Antenna Performance

The relative shapes of the sensor response curves as the footprint traversed land-water interfaces were compared for selected EREP passes. During SL-2, the California Coastline was utilized as the target area, and analysis determined that no antenna degradation occurred during SL-2. The specified target site to perform this task was the Pacific Ocean - Baja California - Gulf of California area. Data was acquired over this site on Skylab pass numbers 27, 28, 38, 81 and 82 during SL-3 and SL-4. Comparison of sensor response curves for these passes and simulation for Skylab pass numbers 27 and 81 ground tracks has revealed that no antenna degradation occurred.

3.5.2 Antenna Resolution

A discussion of the change in antenna brightness per unit area traversed by the antenna beam pattern was provided in Section 7.4 of MSC-05528, Volume VI, using a sample from SL2 pass 1 over the California coastline. This analysis showed the relation between change in area and change in antenna brightness for a typical crossing of a land-water boundary.

3.6 Baseline and Gain Stability (SPE-S194-006)

This task was divided into three major evaluation objectives:

- 1) An evaluation of S194 system precision (standard deviation);
- 2) Evaluation of sun-angle effects on the measured brightness temperature;
- 3) Evaluation of the system output response to sharp transients in brightness temperature at the radiometer input.

No terms appeared in the system transfer equations that were analogous to gain because the Dicke switching was assumed to be faster than any gain variation. Thus, no direct measurement of receiver gain stability was possible with the data available. However, analysis of data standard deviation over homogeneous targets was used to provide at least a coarse measure of gain stability.

3.6.1 Radiometer Stability over Homogeneous Targets

The standard deviation of antenna brightness measurements over selected deep space, the Gulf of Mexico, and Sahara Desert passes were evaluated for each Skylab mission. (See Section 8.1 of MSC-05528, Volume VI, for details.) A summary of the 1σ standard deviation from the selected passes is provided in Table 3.6.1-1. The standard deviation of deep-space measurements was seen to be significantly lower than that for either the Gulf of Mexico or Sahara Desert passes. Although attempts were made to select targets that were as uniform as possible, it was obvious that the larger variations for the Gulf and Sahara sites were due to the nonhomogeneity of the targets. For the deep-space passes, Skylab was oriented in the solar inertial mode. Therefore, the celestial background filling the antenna pattern remained fixed with time. It was believed that the measured standard deviation seen in the deep-space data, approximately 0.3°K , was due primarily to S194 instrument variations, and that the standard deviation of Gulf and Sahara data was predominately a measure of target brightness fluctuations.

3.6.2 Sun-Angle Error Estimates

The effects of solar input to the S194 antenna measurements can be realized in two different forms:

- 1) Reflection of the sun from water surfaces (sun glint);
- 2) Direct or reflected input from Skylab surfaces to the antenna main beam or sidelobes.

From an examination of design and installation provisions (see Section 8.2.1 of MSC-05528, Volume VI), it was concluded that reflected input from Skylab surfaces to the major portion of the hemispherical antenna pattern were effectively eliminated by mounting and considerations of clear field of view. Also, antenna design reduced sidelobe and backlobe levels to a degree that direct or reflected input would not provide a significant contribution to antenna brightness measurements during the earth viewing data orientation. There have been no apparent effects on in-flight measured brightness that could be attributed to direct solar input to the antenna sidelobes, or from reflections from Skylab structure or attached hardware into the S194 antenna main beam or sidelobes. However, theoretical analysis showed that solar reflections from sea surfaces could provide a significant alteration of measured sea brightness for sun elevation angles greater than about 60 degrees. The effects of sun glint on brightness measurements were readily apparent from a number of ocean sites viewed at high sun angles, although the magnitude of the increase in brightness was only about half of that expected.

Table 3.6.1-1 Antenna Brightness Standard Deviation over Selected Homogeneous Targets

TARGET SITE	SKYLAB MISSION	NUMBER OF SAMPLES	ONE SIGMA STANDARD DEVIATION ($^{\circ}$ K)
Deep Space	SL2	3321	0.30
	SL3	831 2055	0.38 0.15
	SL4	2889 2883	0.30 0.32
Gulf of Mexico	SL2	360 273	0.70 0.68
	SL3	318 161	0.76 0.84
	SL4	320 327	0.70 0.93
Sahara Desert	SL2	NA	NA
	SL3	293 386	1.72 0.78
	SL4	213	1.18

3.6.3 Radiometer System Time Response

The SL94 system response, as measured by the Y-factor digital output, was evaluated to determine the time required for data to stabilize after a sharp change in input antenna brightness, or a sharp change in input to the receiver, such as during calibration-mode changes. This evaluation was made to determine whether large ground temperature transitions, such as a land-sea boundary, would produce oscillations in the output data. It was also necessary to verify that the Y-factor data would stabilize rapidly after mode change to ensure a valid in-flight calibration. This concern for Y-factor stability was based on a problem experienced during preflight integration testing at Denver and St. Louis. The results of this evaluation are in Section 8.3 of MSC-05528, Volume VI, and show that there are no oscillatory tendencies in the data, and further, that instrument response time was adequate to faithfully reproduce temperature fluctuations at the input to the receiver.

3.7 Radiometer Combined Insertion Loss (SPE-SL94-007)

This section summarizes the assessment of radiometer combined insertion loss.

3.7.1 Qualification of Deep-Space Brightness

Deep space temperature in the L-band is accurately known. Therefore, deep space was frequently used as a calibration source for evaluating SL94 antenna brightness data. To ensure that the area of the celestial sphere viewed during deep-space passes was free from "hot spots" that could alter the nominal background brightness temperature, plots of the SL94 antenna pattern were projected on a celestial map, together with the sun and moon positions. The antenna pattern was convolved with surveys of the galactic plane and the moon to provide estimates of brightness increases due to their influence. This analysis showed that the contribution of the galactic plane was negligible (less than 0.1°K , worst case) and that the lunar contribution was a maximum of approximately 0.25°K with the moon centered in the antenna FOV. See Section 9.1.3.1.1 of MSC-05528, Volume VI, for details of the cosmic background calibration.

3.7.2 System Calibration from SL2 Deep-Space Data

The first deep-space pass (during SL2) provided a mean measured brightness temperature considerably higher than expected. The error was considered too great to be accounted for by uncertainties in the insertion loss terms, and was therefore attributed to errors in the radiometer electronics-box calibration. The system transfer equations contain two "calibration constants", C_2 and C_4 , which could only be derived by system

measurements. These two calibration constants were believed to be in error. The system transfer equations were therefore re-evaluated using a known value for deep space brightness and some preflight hot calibration test data as two absolute calibration sources. Simultaneous solution of the system equations using the two calibration sources as known inputs resulted in new values for C_2 and C_4 . The new calibration constants "forced" the system equations to provide the expected antenna brightness for deep space. See Sections 9.1.3.1.2 and 9.1.3.1.3 of MSC-05528, Volume VI, for details of this recalibration procedure. Revisions to the JSC PDP programs* were made before SL2 SL94 flight data processing to incorporate the new values for calibration constants. The constants based on this SL2 re-evaluation were applied to the data processing for all three missions. (See appendix A, Section II for an alternate calibration procedure.)

3.7.3 Insertion Loss Evaluations

Between the antenna aperture and the point in the radiometer electronics at which the Dicke switch compared the antenna temperature with the reference load, there are transmission line components. Signal attenuation from these components, and their physical temperature, modified the measured antenna temperature. Thus, evaluation of these loss terms, their physical temperature, and their consistency throughout the flight was required. This was especially true for the SL94 because it used a coaxial cable between the electronics box and the antenna and used a corporate feed structure to feed the planar-array antenna. SL94 insertion loss terms and electronics-box calibration constants were all interdependent; i.e., some fixed value for one must be assumed in order to evaluate the others. Calibration constants (see paragraph 3.7.2) were evaluated assuming that all insertion loss terms were unchanged from their preflight established values. Individual insertion loss terms were evaluated, as summarized in the following paragraphs, while assuming the electronics-box calibration constants were held constant.

3.7.3.1 Insertion Loss Check from Data Repeatability - Comparison of the mean value of measured brightness from all deep-space passes from SL2, SL3, and SL4 was used in the interim sensor performance evaluation report (MSC-05528, Volume VI) to show that there had been no significant change in the insertion loss throughout the Skylab flight period. Mean values of antenna brightness from the five deep-space passes compared to within less than 3°K , and there was no indication of any degradation of sensor operation or trends in the values obtained. The absolute values obtained for the Gulf of Mexico and Sahara Desert sites as part of the linearity evaluation (paragraph 3.4.3.2) also demonstrated consistent sensor operation throughout the three Skylab missions.

*Earth Resources Production Processing Requirements for EREP Electronics Sensors, PHO-TR524, NASA/JSC, 3 January 1974.

3.7.3.2 Verification of Antenna Pattern - The theoretical response of the S194 antenna brightness based on a surface model was compared to the measured brightness for several passes over land-water interfaces to evaluate degradation of antenna pattern from preflight to in-flight. The theoretical response was generated by convolving a computer model of the preflight antenna pattern over a surface model of the land-water interface. The surface model used straight-line sections for boundary lines of regions of different assumed brightness temperatures along the Skylab ground track. The comparison of the theoretical response to the measured data, especially in the vicinity of the transition region between land and water, was used to verify antenna integrity. The evaluation of selected SL2, SL3 and SL4 target sites is detailed in Appendix E, MSC-05528, Volume VI. The results indicated no apparent degradation of antenna pattern. Verification of the antenna pattern provided an indication that no change in the corporate feed structure of the antenna had occurred, and it was assumed that the insertion loss of the feed was also unchanged.

3.7.3.3 Insertion Loss Evaluation by Investigation of Individual Loss Terms - The error in absolute brightness of selected data was used to evaluate individual insertion-loss terms. For this analysis, it was assumed that the total error was due to insertion loss; and the calibration constants were assumed to be unchanged from their values computed after SL2. For this analysis, the error in brightness was to be the difference between the measured antenna brightness and the value obtained from the target simulation model. Insertion loss terms consisted of RF cable loss factor, L_{CA} , antenna to antenna RF cable mismatch, Γ , and antenna assembly loss factor, L_A . The analysis took each loss term individually and assessed the change in each term required to account for the indicated error in measured brightness. These analyses are in Sections 9.1.3.2 and 9.1.4.1 of MSC-05528, Volume VI. The results of this analysis, although not conclusive, provided strong indications that the errors in measured brightness were not due to errors in insertion loss values. This was inferred by the unreasonable changes in loss terms required to provide the requisite change in measured brightness.

3.7.4 Thermal Effects on Insertion Loss Error Estimates

The measured data response over a homogeneous target was evaluated to determine whether temperature changes of loss components occurring throughout the pass were properly compensated for in the system equations. (See Section 9.2 of MSC-05528, Volume VI.) This analysis was most readily accomplished using a deep-space pass, where the target temperature could be assumed to be uniform. The analysis showed that the corrections applied to the data as a result of the temperature changes provided a resultant antenna brightness that was reasonably stable, indicating that the thermal corrections were of the proper magnitude. No cumulative error was apparent in the long deep-space passes. The largest variations in the resultant

antenna brightness were due to the coarseness of the Y-factor changes. Therefore, the temperature corrections for insertion loss components were nearly masked by the Y-factor digital resolution. The sensitivity of antenna brightness to individual loss component temperature changes was also examined to determine what level of uncertainty could be tolerated in these temperature measurements without a significant uncertainty in antenna brightness. This analysis verified that, for typical passes, the uncertainty in antenna brightness due to temperature changes would be considerably less than the instantaneous resolution of the radiometer.

4. FINAL RESULTS

The general performance of the S194 L-Band radiometer was satisfactory throughout almost the entire preflight test program and the three Skylab missions. However, there were a few anomalies that affected a small amount of the S194 data. Table 4-1 provides S194 system anomalies experienced during the Skylab missions. The table is limited to those anomalies that resulted in erroneous or questionable data, or that required corrections be made in data processing to correct for the anomalous condition.

One anomaly not included in Table 4-1 is the cold-load operating range. An expected range of 200 to 250°K was established as the nominal expected operating temperature range for the two cold loads. Both of the loads operated above the upper range for a majority of the EREP passes. However, unless both cold loads exceeded the limit condition of zero bit counts in the output data stream (269.4°K for cold load #1, and 256.7°K for cold load #2), a valid calibration could still be performed.

There were two other types of anomalies that appeared at random in the data, the EMI-induced anomalies and the data processing anomalies. In both cases, the anomaly is characterized by atypical changes in measured antenna brightness for short periods. These data anomalies affect only a very small percentage of the data and are easily recognized.

Table 4-1 S194 Flight Data Anomalies

EREP PASS	ANOMALY DESCRIPTION	EFFECTS ON SYSTEM OPERATION
All EREP Passes	Enclosure temperature (t_D) was consistently below its design temperature (297°K). Even though the enclosure monitor exhibited a gradual temperature rise during every pass, the design temperature was never reached. The enclosure heaters were apparently inadequate.	Systems equations for S194 are based on an assumed constant value for enclosure temperature throughout each pass. Because the enclosure temperature showed a general warming trend during all EREP passes, a correction must be made to the computed value of antenna brightness. A correction term has been included in the PHO-TR524 production data processing system. Rationale & discussion of the development of this correction term are in Section 3.2.2.3 of the sensor performance report MSC-05528, Vol VI, dated September 6, 1974.
SL2 Passes 1, 2, 3, 4, 5, 6, & 9. SL3 Pass 45	Hot RNG thermal temperature (T_{SH}) was low for a portion of each of the indicated passes. The low temperature of the hot RNG is attributed to low enclosure temperature, thus requiring a longer warmup time for the hot RNG heater to achieve stable operating range.	A change in hot RNG temperature will result in a change in system gain. To offset this error, a correction is required to the calculation of antenna brightness. This correction term has been developed & is outlined in Section 3.2.2.3 of the sensor performance report MSC-05528, Vol VI, dated September 6, 1974. This correction is <u>not</u> included in the PHO-TR524 production data processing system, & must be made manually by each data user.

Table 4-1 (Concluded)

EREP PASS	ANOMALY DESCRIPTION	EFFECTS ON SYSTEM OPERATION
SL3 Passes 43, 46 & 52 SL4 Passes 80, 83 (Part 2), 89, 90, 91, 92 & 93	Both cold-load RNG thermal monitors (T_{SC}) exceeded their upper temperature limit (0 bit count in digital data output) before postpass calibration. On pass 80 & pass 83 (Part 2: GMT 16:55:00 to 17:04:00), both cold loads reached limit conditions before prepass calibration, thus making the entire data period unusable.	When both cold-load thermal monitors exceed their upper temperature limit, the true thermal temperature of the cold calibration source cannot be determined. This results in an invalid calibration & thus, erroneous values for processed brightness temperature data. Computer software programs have been generated to permit reprocessing data such as this by using valid calibration data from other time periods. However, the accuracy of this procedure has not been verified.

5. CONCLUSIONS

In spite of some data problems arising from enclosure heater and internal calibration data anomalies, the performance evaluation has shown that the S194 radiometer provided data that compares well with predicted response so long as suitable corrections are applied to the data. The following conclusions can be drawn with respect to specific characteristics observed in hardware performance and design.

5.1 Housekeeping and Internal Calibration Data

Except for specific anomalies noted in Section 4, housekeeping and calibration data generally fell within expected limits and showed no tendency to drift or shift in value; thus indicating that good health and integrity of the electronics systems was maintained throughout the mission. Based on the excellent stability of radiometric data during all deep-space passes, it is concluded that the frequency of calibration was adequate. However, the change in mean brightness following calibration updates would suggest that the inaccuracies of the internal calibration were not negligible. They were found to result in step changes of up to 2°K at deep-space temperatures, although the potential error would be considerably less at higher brightness temperatures.

5.2 Radiometric Data

A small amount of flight data was lost, or is of questionable accuracy due to thermal limits being exceeded on the internal calibration sources. However, the data lost were only a very small percentage of the total data available. There was no evidence of any S194 performance degradation resulting from damage, aging or deterioration of the S194 hardware. However, there was some degradation and loss of data resulting from thermal design deficiencies coupled with environmental extremes present throughout the three Skylab missions. There was no indication that instrument accuracy was degraded as long as one of the two cold loads operated within the measurable range of its thermal monitor.

5.3 Antenna Integrity

There were no S194 hardware failures during the Skylab mission. However, there was some concern about antenna integrity after review of SL2 and SL3 photographs showing the S194 antenna cover bulged outward. Coastline data were used to evaluate the antenna pattern. This analysis has shown no apparent degradation of the antenna pattern from its preflight measured response. Definitive values for antenna insertion losses could not be determined directly from evaluation of the flight data because the electronics-box calibration was suspected to be in error. Also, preflight end-to-end calibration tests were not possible, so that verification during system test could not be done. However, it was shown in the sensor performance evaluation that it would require unreasonable changes in the values of insertion loss to account for the errors observed in the antenna brightness data. Use of the preflight-determined values for insertion loss from acceptance tests, in conjunction with recomputed electronics-box calibration constants, provided good linearity and absolute accuracy from the S194. The excellent repeatability of measured brightness throughout the Skylab missions has shown that insertion loss did not change during flight.

6. RECOMMENDATIONS

Based on the results and conclusions from the sensor performance evaluation of the S194 instrument, the following recommendations are offered for subsequent programs:

1) Increased use of a down-link data transfer system for near-real-time evaluation is recommended for both in-flight scheduling and hardware performance evaluation purposes.

2) A computer simulation of the sensor, including all loss terms in the calibration and antenna paths, is recommended. It would be desirable to have this model during preflight system test for both its verification and the determination of additional tests required before flight.

3) The radiometer design technique of digitally attenuating the input signal reduced instrument noise levels to insignificant levels and permitted the measurement of very low input signal levels as well as the highest signal levels that naturally occurring targets will present to the sensor. It is recommended that this design technique be utilized in future radiometer instruments. Also, a necessary recommendation is that the internal calibration sources and the internal switching between input signal and calibration sources are a definite requirement for all radiometers. The design and control of the hot load internal calibration source was excellent. The design of the cold load calibration source could be improved. This improvement could be performed in either of two ways. The first method would be to have better control over the value of the cold load (smaller range of variation), or the second method would be to retain read-out accuracy but increase the read-out dynamic range. This could be accomplished by increasing word-size or by using multiple, overlapping dynamic ranges with one bit used to designate the range used and having instrument logic select the optimum range. It is not important that the cold load never vary but it is important that the cold load value change slowly ($<1^{\circ}\text{K}$ per hour) once it reaches the usable range and that it be known. The nominal value of the cold load should be near (preferably below) the 90°K to 100°K brightness temperature of the ocean rather than the 250°K value of S194.

4) It is recommended that the digitizing steps within the radiometer be decreased to improve the sensitivity. This could be performed by increasing the binary representation of the output of the radiometer from a 10-bit word to a 16-bit word.

5) Elapsed time generated internal to the sensor and recorded with the scientific and engineering data is recommended to alleviate timing problems encountered in data processing of the S194 flight data.

6) End-to-end system calibration, including thermal and space environment simulations must be performed. These were not performed on the S194 prior to launch and would have uncovered the fact that the enclosure heaters were inadequate for the programmed warm-up time in a space environment.

7) Two of the limitations of the S194 radiometer were the small physical size of the antenna (large footprint area) and the fixed nadir viewing angle of the antenna. In order to decrease the size of the footprint, the physical size of the antenna should be increased, however, increasing the size of the present S194 antenna ($\approx 1\text{m. square}$) prohibits the possibility of physically scanning the antenna at the required rates. It is recommended, therefore, that for future L-band radiometers the technique of utilizing a phased-array antenna mounted in a semicircle $\pm 45^\circ$ from nadir around the cylindrical space vehicle be employed. In this manner, the required large size antenna for greater resolution, may be electronically scanned to produce a mapping of the targets rather than simply an integrated brightness temperature over the large footprint area. The response time of the radiometer would need to be improved if scanning is employed.

8) The final recommendation is that it is necessary to have an on-going Sensor Performance Evaluation task for as long as the instrument is acquiring data. This would include sensor and target simulation models for validity of scientific data, determining corrective factors for operational malfunctions and verification of data processing algorithms.

7. NOTES

7.1 Acknowledgements

The effort covered by this report was sponsored by the Lyndon B. Johnson Space Center, Earth Resources Program Office. It is based on the results of a concerted effort by numerous individuals in NASA, industry, and academic organizations. These include:

The Science and Applications Directorate
NASA, Lyndon B. Johnson Space Center
Houston, Texas

Lockheed Electronics Company, Aerospace Systems Division
Houston, Texas

Ohio State University
Electroscience Laboratory
Columbus, Ohio

Martin Marietta Corporation, Denver Division
Denver, Colorado

Acknowledgement is made to Dr. W. Peake of Ohio State University who provided technical consultation to the Martin Marietta evaluation effort, and contributed significant inputs and technical information used in the SPE reports. We also wish to thank Messrs. T. Flattau and M. Stillwell of the AIL Division of Cutler Hammer who contributed significantly to the understanding of sensor operation peculiarities and malfunction diagnosis.

7.2 Abbreviations

Abbreviations in common usage have been used for English units of measure. International units (SI) have been abbreviated in accordance with E. A. Mechtly's NASA SP-7012, The International System of Units, 2nd Rev, National Aeronautics and Space Administration, Washington, D.C., 1973--except for steradian, which has been abbreviated to ster.

AIL	A division of Cutler-Hammer
C&D	Control and display
CAL	Calibration
CSM	Command and service module
DOY	Day of Year
EIS	End Item Specification
EMI	Electro magnetic interference
EREP	Earth Resources Experiment Package
FOV	Field-of-view
GMT	Greenwich Mean Time
H/K	Housekeeping
ILCA	Inverter Lighting Control Assembly
JSC	Johnson Space Center
KSC	Kennedy Space Center
LEC	Lockheed Electronics Company
MDA	Multiple Docking Adapter
MDAC-E	McDonnell Douglas Astronautics Company - East
MFMR	Multi-frequency microwave radiometer
MMC	Martin Marietta Corporation
NASA	National Aeronautics and Space Administration
NM	Nautical miles
NOAA	National Oceanic and Atmospheric Administration
PDP	Production data processing
RMS	Root mean square
RNG	Reference noise generator
S&AD	Science and Applications Directorate
SPE	Sensor performance evaluation
VSWR	Voltage standing wave ratio
ZLV	'Z' local vertical (Standard vehicle orientation for EREP passes where Skylab Z axis is oriented and maintained along the earth local vertical)

APPENDIX A

I. Evaluation of S194 Radiometric Temperature Error Due to Pointing Uncertainties

SKYBET is a computer printout of selected ephemeris data and S194 field-of-view (FOV) data tabulated as a function of GMT. Due to the large S194 antenna beamwidth, it was not possible to establish the true location of the antenna footprint with respect to time by using S194 measured response over land-water interfaces. Therefore, the accuracy of the S194 pointing tabulations from SKYBET could not be directly verified by evaluation of S194 flight data. However, because the radiometer measurement accuracy was of primary concern, the approach taken was to determine the uncertainty in pointing based on analysis of installation data and Skylab attitude uncertainties, and then to assess the consequent uncertainty in S194 antenna brightness-temperature measurement.

A. Sensor Installation and Skylab Attitude Uncertainties

The SKYBET determination of sensor pointing includes corrections for known offsets in sensor alignment and vehicle attitude. However, due to mechanical alignment tolerances and electronic equipment operation tolerances, there were other potential offsets in sensor pointing that resulted in some uncertainties in the SKYBET data provided for the center of FOV. Mechanical alignment of the antenna to the spacecraft was measured directly during preflight alignment checks. Estimated uncertainties in these preflight measurements were less than 0.2 degrees about the Skylab X and Y axes, which were considered negligibly small compared to the antenna beamwidth (approximately 15 degrees at the half-power points).

No direct measurements of Skylab attitude errors were made before flight. However, there have been several analytical studies to demonstrate Skylab's ability to satisfy its requirements for attitude control orientation.

An analysis of the total cumulative uncertainty in the knowledge of attitude pointing accuracy was performed by the JSC Mathematical Physics Branch. A summary of the results of this study, applicable to the EREP S190A and S192 sensors, is in memorandum FM81 (73-274) from Emil R. Schiesser of the JSC Mathematical Physics Branch, to Mr. Paul Norris, Martin Marietta, dated November 1, 1973. The errors presented in this memorandum for S190A and S192 also apply to S194 because the sensor-dependent error sources were negligible, as discussed above.

From this analytical study, data for S194 could be expected to provide vehicle attitude and sensor FOV pointing data with 3σ uncertainties as follows:

Skylab Pass	3σ Skylab Attitude Pointing Error ($^\circ$)	S194 Center of FOV Location Error on Earth Surface (n mi)
Solar Inertial Passes	0.4	1.5
EREP ZLV Passes 1 through 20	2.5	10.2
EREP ZLV Passes 21 & after	0.8	3.2

B. Estimate of Radiometric Temperature Error Due to Pointing Uncertainties

The technique used to estimate the effects of pointing error on the accuracy of the S194 radiometric data can best be explained by an example that demonstrates the technique applicable to a near-worst-case uncertainty in pointing error, and a worst-case target situation at a sharp brightness-temperature transition. In this example, the radiometric temperatures of the land and water were assumed to be 300°K and 100°K , respectively, with the pointing error at the land-water interface, as shown in Figure A-1.

This simplified model assumed that the antenna accepted energy only from targets in the main beam. Because the efficiency of the S194 antenna was very high ($>97\%$), this assumption should not have significantly altered the results of the analysis.

In Figure A-2, the antenna main beam was divided into concentric 1-degree increments, with the pattern factor for each segment indicated. The antenna temperature was computed by weighting the target temperatures by their areas and the appropriate antenna pattern factors.

Using this example, the worst-case error of 2.23 degrees in pointing, when applied to the assumed target model, gave an error in the measured brightness temperature of 0.21°K (i.e., S194 would measure 100.21°K versus the assumed 100°K).

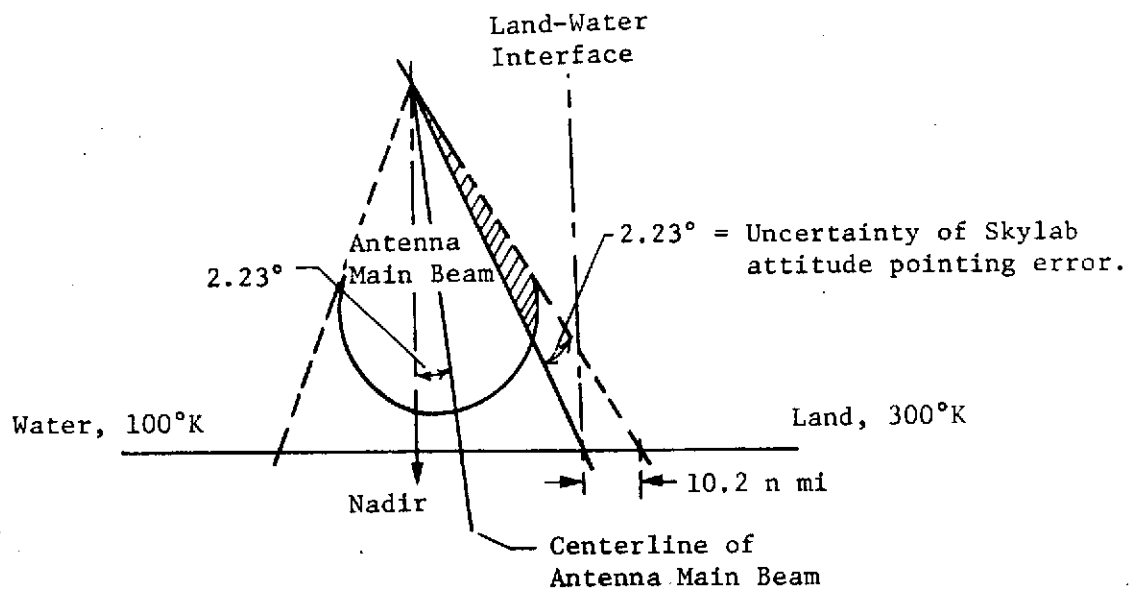


Figure A-1 S194 Antenna Pattern

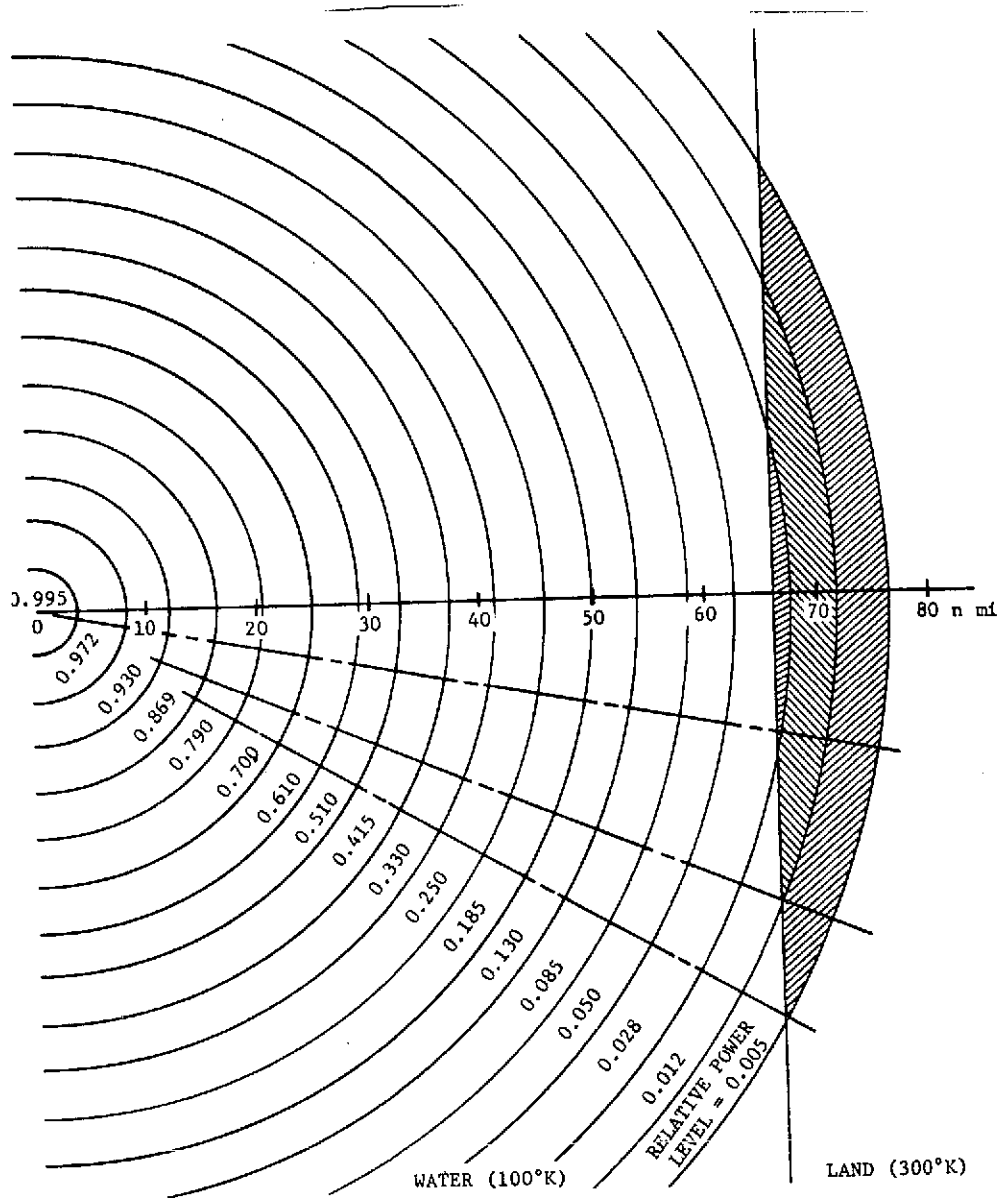


Figure A-2 Effects of Pointing Error on Radiometer Accuracy

II. Skylab S194 Radiometer Calibration

The radiometer system for the S194 experiment was designed to measure the absolute brightness temperature of the radiation incident on its antenna from the nadir direction. However, because the vehicle operated in a different environment from that in which the original calibration tests were made, because the internal environment of the radiometer system departed from the nominal design values, and because the data processing procedure used only those calibration data preceding a given set of measurement data, there are a number of uncertainties in interpreting the processed output of the instrument. The purpose of the analysis that follows is to describe the source of some of these uncertainties, and to indicate some possible approaches to minimizing certain of them. The problem falls into two parts--the first concerned with the relationship between the incident antenna brightness, T_{AC} , and the antenna temperature as measured at the Dicke switch, T_{PA} , referred back to the antenna terminals, T_{SA} . The second part concerns the internal calibration of the radiometer, as it is influenced by drifts in the physical temperature of the various components in the time interval between a calibration and a data measurement.

A. Relationship between T_{AC} , T_{SA} , and T_{PA} *

A schematic of the transmission system between the antenna and the Dicke switch is shown in Figure A-1 and a flow graph representation in Figure A-2. Assuming that the noise powers generated in the receiver, the antenna, and the cable are incoherent, and that a reference bandwidth, Δf , is chosen so that a noise power is directly equal to the corresponding noise temperature, the values of the two upper nodes in Figure A-2 represent $\sqrt{T_{SA}}$ and $\sqrt{T_{PA}}$, respectively.

The values of the scattering parameters entering the upper left and lower nodes are given by

$$a_1 = \frac{2(T_A \gamma_A R_o)^{1/2}}{(Z_a + R_o)} \quad (A-1)$$

$$a_2 = \frac{2(T_R \gamma_B R_o)^{1/2}}{(Z_b + R_o)} \quad (A-2)$$

$$T_{L1} = (1 - L_{CAB}) t_D + (1 - L_{CAA}) L_{CAB} t_{CAA} \quad (A-3)$$

$$T_{L2} = (1 - L_{CAB}) L_{CAA} t_D + (1 - L_{CAA}) t_{CAA} \quad (A-4)$$

where

R_o = characteristic impedance (real) of cable

$$Z_a = r_a + jx_a = \frac{(1 - \Gamma_A)}{(1 + \Gamma_A)} \quad \text{antenna impedance}$$

$$Z_b = r_b + jx_b = \frac{(1 - \Gamma_B)}{(1 + \Gamma_B)} \quad \text{receiver impedance}$$

$\Gamma_A \Gamma_B$ = complex reflection coefficients

$e^{-\gamma \ell}$ = transmission coefficient of cable

$$|e^{-\gamma \ell}|^2 = L_{CA}$$

* Unless explicitly noted, all variables used in this section are as defined in Table 9.1.3.1.2 and Section 5.1.1 of MSC-05528, Volume VI.

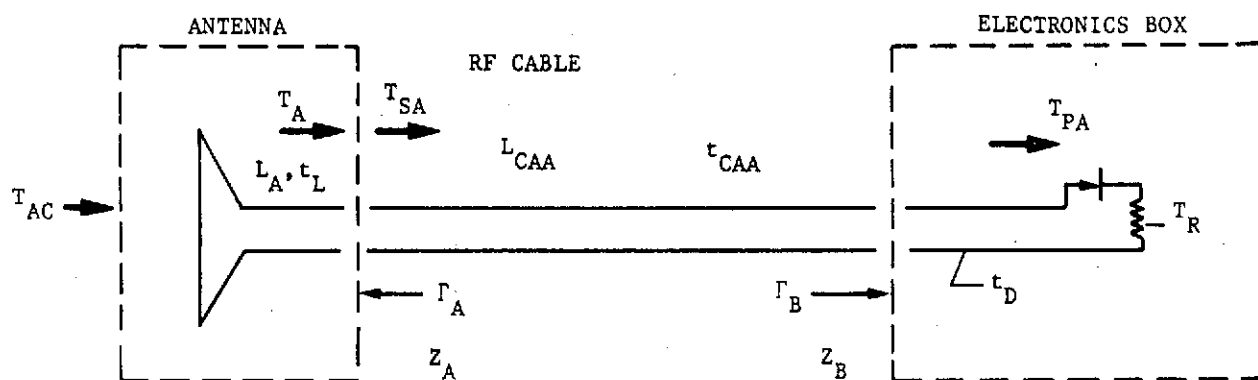


Figure A-1 Antenna to Dicke Switch Schematic

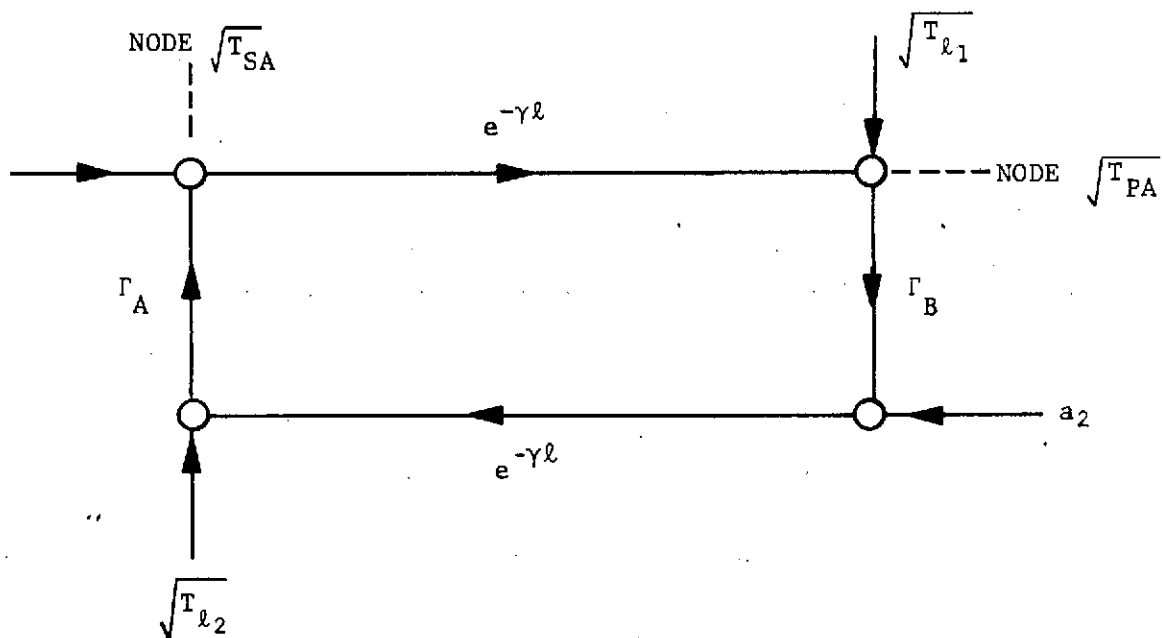


Figure A-2 Simplified Flow Diagram

T_A = noise temperature of noise power antenna would deliver to a conjugate match load

T_R = noise temperature of power that the receiver input terminals would deliver to a conjugate match load

From the flow graph, it is seen that

$$T_{SA} = \left[\frac{1}{S} T_A \left(1 - |\Gamma_A|^2 \right) + \left| \Gamma_A e^{-\gamma \ell} \right|^2 T_R \left(1 - |\Gamma_B|^2 \right) + \left| \Gamma_A \right|^2 T_{\ell_2} + \left| \Gamma_A \Gamma_B e^{-\gamma \ell} \right|^2 T_{\ell_1} \right] \quad (A-5)$$

$$T_{PA} = \frac{1}{S} \left[\left| e^{-\gamma \ell} \right|^2 T_A \left(1 - |\Gamma_A|^2 \right) + \left| \Gamma_A e^{-\gamma \ell} \right|^2 T_R \left(1 - |\Gamma_B|^2 \right) + T_{\ell_1} + \left| \Gamma_A e^{-\gamma \ell} \right|^2 T_{\ell_2} \right] \quad (A-6)$$

$$S = \left| 1 - \Gamma_A \Gamma_B e^{-\gamma \ell} \right|^2 \quad (A-7)$$

These are the equations that could replace Equations 5.1.1-14, 5.1.1-27, and 5.1.1-28 in Section 5 of the sensor performance report, MSC-05528, Volume VI. For the S194 radiometer, neither the complex reflection coefficients Γ_A and Γ_B nor the transmission factor $e^{-\gamma \ell}$ nor the noise temperature T_R delivered to the line by the receiver input terminals is known. However, it is known that $|\Gamma_A| \cong 1/9$, $|\Gamma_B| \cong 1/40$, $\left| e^{-\gamma \ell} \right|^2 = L_{CA}$, and it can be assumed that $T_R = t_D$, the electronics box physical temperature, or more precisely $T_R = t_D + T_e$ where T_e is an excess noise, because most semiconductor components generate noise temperatures in excess of that delivered by their Thevenin equivalent circuit.

The majority uncertainty caused by the known VSWR in the cable is due to the multiplying term, $1/S$, which can vary between 0.9946 and 1.0054. Thus, the uncertainty in T_{AC} is on the order of $\pm 0.0054 T_A$, i.e., about $\pm 1/2^\circ K$ over water and $\pm 1-1/2^\circ K$ over land. In addition, if $T_R = t_D + T_e$, the increase in T_{SA} is about $T_e/90$, independent of T_{SA} . Uncertainties of both types are essentially corrected for by the change in constants C_2 and C_4 , because a change in C_2 produces

a change in T_{SA} essentially independent of T_A , while a change in C_4 produces a change in T_{SA} that is proportional to T_A . The values of C_2 and C_4 were evaluated after the SL2 mission, as discussed in Section 3.7.2 of this volume. Thus, the uncertainty in the receiver/cable/antenna mismatches (Γ_A, Γ_B) and the receiver electronics noise level (T_R) is compensated for by the in-flight calibration of the receiver transfer function.

B. Calibration - The Balance Equations

The second type of uncertainty that was not corrected for in the original calibration procedure is due to the difference between the design values of the enclosure temperature, t_D ; the hot-load source temperature, T_{SH} ; and the cold-load source temperature, T_{SC} ; respectively, and those actually encountered, and to the drift in these variables between the time of a calibration and the time of a data measurement. To determine the nature of these uncertainties, consider the equations governing the radiometer operation at calibration (See Figure B-1). For measurement of hot load:

$$G' \left(T_e' + T_{PH}' \right) = A_H \left(T_e' + T_{PR}' \right) \quad (B-1)$$

And for measurement of cold load:

$$G' \left(T_e' + T_{PC}' \right) = A_C \left(T_e' + T_{PR}' \right) \quad (B-2)$$

from which:

$$T_e' = -T_{PR}' + G' \left(\frac{T_{PH}' - T_{PC}'}{A_H - A_C} \right) \quad (B-3)$$

where the prime (') indicates the value of a variable at the time a hot or cold calibration is made, and

A_C = digital output value of radiometer during cold calibration

A_H = digital output value of radiometer during hot calibration

G' = differential gain of antenna channel with nominal value
1/1.01

T_e' = receiver noise temperature referred to Dicke switch

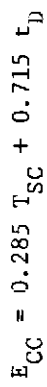


Figure B-1 Diode (Dicke) Switch

T_{PR}' = reference-load noise-temperature referenced to Dicke switch.

Because the reference load and the hot load have nearly identical construction, and are monitored by a common thermocouple, it is assumed that $T_{PR}' = T_{PH}'$. At the time of a measurement,

$$G (T_e + T_{PA}) = A_A (T_e + T_{PR}) \quad (B-4)$$

and again it is assumed that $T_{PR} = T_{PH}$.

The receiver noise and the differential gain may depend on t_D , so that one may write

$$T_e = T_e' + \alpha \tau_D + \beta \quad (B-5)$$

$$G = G' + \gamma \tau_D$$

$$\tau_D = t_D - t_D' \text{ (drift in box temperature)}$$

where α , β , and γ are unknown "constants," although, as will be seen below, analysis of SL2 and SL3 data indicates that β , the "constant" representative of the excess receiver noise appears to depend on the cold-load source temperature, T_{SC} , i.e., is actually a variable.

After some manipulation, assuming that the loss in the line from reference load to Dicke switch is L_{CH} , and dropping some second-order terms, the equations corresponding to the nominal calibration procedure, Equation 5.1.1-3 in MSC-05528, Volume VI may be found, namely:

$$T_{PA} = T_{PC}' + \frac{(A_A - A_C)}{(A_H - A_C)} (T_{PH}' - T_{PC}') + F \quad (B-6)$$

where:

$$F = -(\alpha \tau_D + \beta) + A_A \left[\alpha \tau_D + \beta - \alpha \tau_D \frac{(T_{PH}' - T_{PC}')}{(A_H - A_C)} + b_1 \tau_{SH} + b_2 \tau_D \right] \quad (B-7)$$

where

$$\left. \begin{aligned} \tau_{SH} &= T_{SH}' - T_{SH} \\ b_1 &= L_{CH} + (1 - L_{CH}) (0.157) \\ b_2 &= (1 - L_{CH}) (1 - 0.157) \end{aligned} \right\} \begin{array}{l} \text{nominal} \\ \text{A-11} \end{array}$$

Note that τ_{SH} is the difference between the hot reference temperature source at the time of calibration measurement and any data (antenna) measurement. The physical temperature of the internal cable between the hot load and the Dicke switch is given by the empirical relation $t_{SH} = 0.157 T_{SH} + 0.843 t_D$, as shown in Figure B-1. Thus assuming that the antenna temperature at the Dicke switch, T_{PA} , can be related to T_{SA} by Equation 5.1.1-14 in MSC-05528, Volume VI instead of the transformation of Equations A-5 and A-6, one obtains

$$T_{SA} = C_1 T_{SC}' + C_2 + \frac{(A_A - A_C)}{(A_H - A_C)} (C_3 T_{SH}' - C_1 T_{SC}' + C_4) + \frac{C}{L_{CA}} \quad (B-8)$$

where

$$C_1 = L_{CC}/L_{CA}$$

$$C_3 = L_{CH}/L_{CA}$$

$$C_2 = \frac{1}{L_{CA}} \left[(t_D' - T_{SC}') (1 - L_{CCB}) + (1 - L_{CC}) t_{CC}' + (1 - L_{CA}) t_{CA} \right] \quad (B-9)$$

$$C_4 = \frac{1}{L_{CA}} \left[(1 - L_{CH}) t_{CH}' - (t_D' - T_{SC}') (1 - L_{CCB}) - (1 - L_{CC}) t_{CC}' \right] \quad (B-10)$$

$$C_5 = (A_A - 1) (\alpha \tau_D + \beta) + A_A (b^1 \tau_{SH} + b^2 \tau_D) - \frac{A_A}{A_H - A_C} (T_{SH}' - T_{SC}') \gamma \tau_D \quad (B-11)$$

This particular form of the equations for T_{SA} was determined before flight, and at that time, C_2 and C_4 were treated as constants, this was based on the assumption that conditions were essentially the same during the preflight calibration, during any in-flight calibration, and during the measurement time. However, the values of the "constants" C_2 and C_4 in the original calibration were not based on Equations B-9 and B-10

because the attenuations and other internal conditions were not considered to be known with sufficient accuracy. Instead C_2 and C_4 were determined from preflight calibration using a reference temperature source that did not present the same reflection coefficient, Γ_A , as the antenna. It is clear from Equations B-9 and B-10 that C_2 and C_4 are not constants, but should be written in the form

$$C_2 = C_{2R} + (C_2' - C_{2R}') \quad (B-12)$$

$$C_4 = C_{4R} + (C_4' - C_{4R}') \quad (B-13)$$

Here, C_{2R} and C_{4R} are empirically determined constant numeric values based on SL4 flight data (currently estimated to be 14.425 and 17.995, respectively, and referred to as the calibration constants C_2 and C_4 elsewhere in this report) and $(C_2'$ and $C_{2R}')$ is the difference between the value of Equation B-9 at a calibration time preceding any data of interest, and the value of Equation B-9 at the particular calibration time associated with those measurements on which the estimate of C_{2R} is based. (Similarly for C_4). The value of C_5 cannot be estimated because the parameters α, β, γ defined in Equation B-11 are unknown.

The above result may be compared to the current processing algorithm used in the JSC production data processing, where:

$$T_{SA} = C_1 T_{SC}' + C_2 + \left(\frac{A_A - A_C}{A_H - A_C} \right) (C_3 T_{SH}' - C_1 T_{SC}' + C_4) - E \quad (B-14)$$

with

$$C_2 = C_{2R} + (1 - L_{CA}) (t_{CACAL} - t_{CA}) / L_{CA} \quad (B-15)$$

$$C_4 = C_{4R}$$

$$E = 0.00243 (370 - T_{SA}) (t_D - t_D'), \text{ and only includes} \quad (B-16)$$

the change in enclosure temperature, t_D .

$$t_{CACAL} = 270.18^\circ K \quad (B-17)$$

Alternatively, E may be replaced by the AIL derived corrections
 $E = E_1 + E_2$ (See Section 3.2.2.3 of MSC-05528, Volume VI.), which accounts
 for both the change in enclosure temperature, t_D , and hot load temperature,
 T_{SH} , with:

$$E_1 = 0.0023 \left(373 - T_{SH} \right) \left(T_{SH}' - T_{SA} \right) \quad (B-18)$$

$$E_2 = \left(t_D - t_D' \right) \left(370 - T_{SA} \right) / \left(324 + t_D' \right) \quad (B-19)$$

Note that terms of the type $\left(T_{SH}' - T_{SA} \right) \left(373 - T_{SH} \right)$ or $\left(370 - T_{SA} \right) \left(t_D - t_D' \right)$ are approximately equivalent to $\left(T_{SH}' - T_{SC}' \right) \left(1 - A_A \right) \left(t_D - t_D' \right) / \left(A_H - A_C \right)$ and thus the E_1 and E_2 corrections correspond to similar terms in C_5 as seen in Equation B-11.

By comparing the procedures that lead to Equations B-8 to B-13, with those leading to Equations B-14 to B-17, it is seen that the recommended algorithm, Equation B-14, accounts explicitly for the variations in t_{CA} , the RF cable temperature and lumps all other corrections for the variation of operating temperatures (particularly those occurring in C_5) in the single term E.

The test of a correction procedure is that it should give the same result for T_{AC} , the incident antenna brightness, using the prepass calibration, as it does using the postpass calibration, i.e., the measured target temperature should be independent of the time of acquisition of calibration data used in the data reduction. A number of data points from passes on DOY 150 (three calibration times), DOY 215, and DOY 216 (two calibration times) indicate that discrepancies of 1 to 3°K between pre-cal and post-cal values of T_{SA} occur.

Some of this discrepancy must be ascribed to quantization errors in determining the data output values for the hot, cold, and antenna measurements, A_H , A_C , and A_A . However, it is likely that some of the discrepancy is due to the fact that C_2 and C_4 are really functions of T_{SC}' , T_{SH}' , etc, and that there may be other types of drift from calibration as suggested in the term C_5 . Thus, Equation B-14 used in data processing, has accounted for some of the variations in flight operating conditions but has not been as complete as may be desired, as indicated by the above discussion and as can be seen by comparison of Equations B-14 and B-8.

C. Effect of Cold-Load Temperature on T_e

Further evidence of the need for a more detailed consideration of the effects of τ_{SH} , τ_{SC} , and τ_D on radiometer performance may be obtained from a study of T_e , the receiver noise temperature referred to the Dicke switch. In the original preflight calibration, it was found that the constants C_2 and C_4 depended on which cold load was selected for calibration, viz.,

$C_2 = 3.2$	$C_4 = 3.8$	Cold Load 1
$C_2 = 2.8$	$C_4 = 4.3$	Cold Load 2

The inflight calibration procedure was based on cold load 1 data, because that load was most commonly connected. However, in principle, because the physical temperatures of the cold loads appear to affect radiometer performance i.e., in Equation B-5, T_e is dependent on T_{SC} , different values of C_2 and C_4 should be used when the calibration is based on cold load 2. To illustrate the apparent effect of the cold loads, the effective noise temperature at calibration time, T_e' , was computed from Equation B-3 for 76 calibrations of cold load 1 and 18 calibrations of cold load 2 that occurred during SL2 and SL3. The values of T_e' obtained were found by a least squares analysis to be represented by the equations

$$T_e' = 334.897 + 1.6071 t_D - 1.6144 T_{SC}' \quad (\text{cold load 1}) \quad (C-1)$$

$$T_e' = 276.226 + 1.1350 t_D - 0.8095 T_{SC}' \quad (\text{cold load 2}) \quad (C-2)$$

The standard deviation in T_e' itself was found to be 9.1 and 4.2°K for cold loads 1 and 2, respectively. The standard deviations in the difference between the actual value of T_e' from Equation B-3 and the value computed from the least squares fit via Equations C-1 and C-2 were found to be 3.9 and 3.1°K for cold loads 1 and 2. A plot of the predicted values of T_e' from Equations C-1 and C-2 is shown in Figure C-1. For these data, the mean values were $\bar{T}_e' = 389.1^\circ\text{K}$ and $\bar{T}_{SC1}' = 247.4^\circ\text{K}$, for cold load 1, and for cold load 2, the mean values were $\bar{T}_e' = 396.9^\circ\text{K}$ and $\bar{T}_{SC2}' = 246.7^\circ\text{K}$.

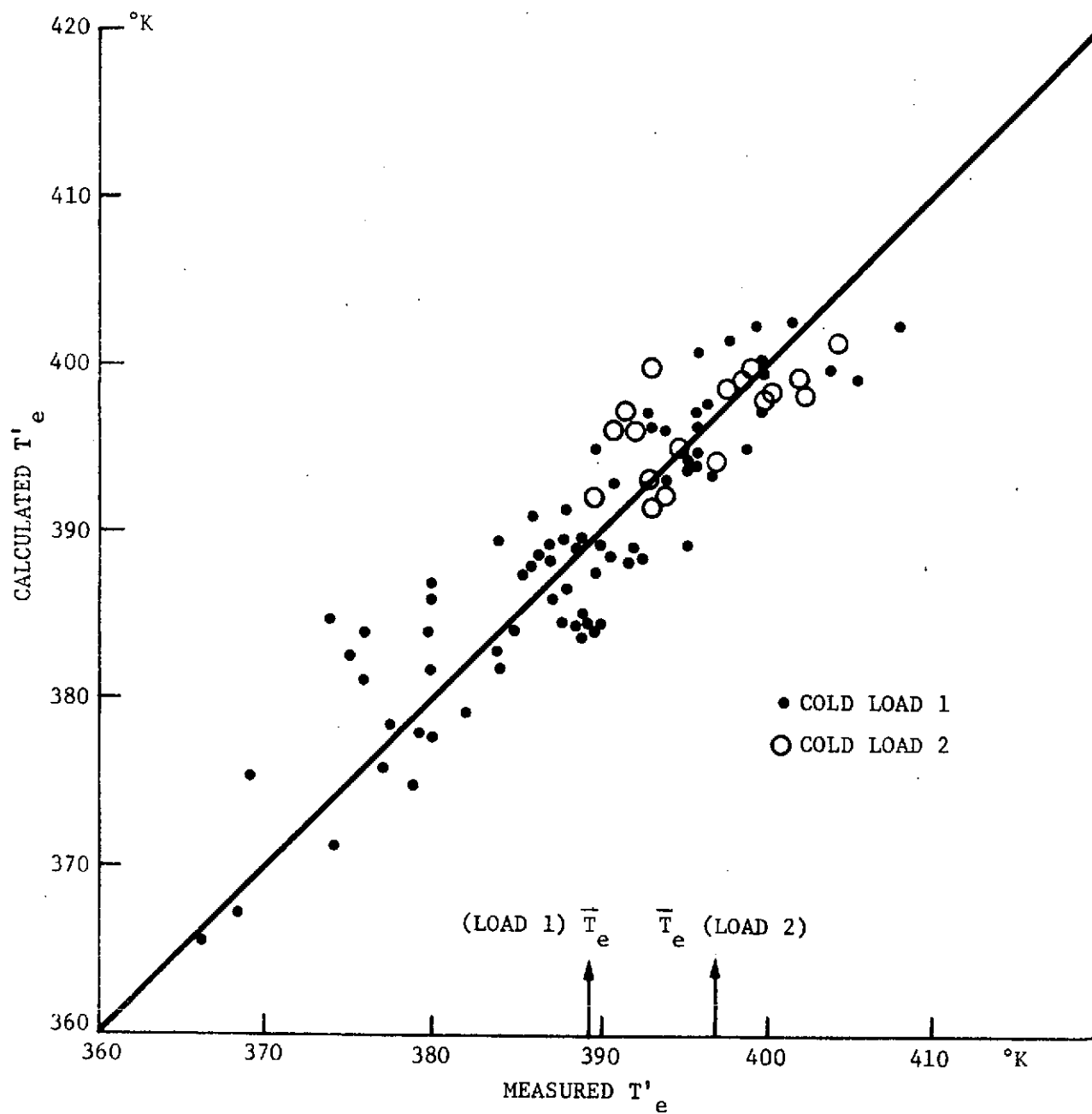


Figure C-1 Measured and Calculated Receiver Noise

Because the noise temperature of a transistor amplifier should not depend on the physical temperature of an external part of the circuit, the linear dependence of T_e' on T_{SC}' indicated by Equations C-1 and C-2 must be an artifact of the computation process. Two possible explanations for this are:

- 1) The constants in the transfer equation used to determine T_{PC} from T_{SC} (Equation 5.1.1-5 of MSC-05528, Volume VI, with $t_{CC}' = 0.285 T_{SC}' + 0.715 t_D'$), which should include the effects of the diode switch, are different for the two different cold-load cables;
- 2) The thermal gradient in the cables from the cold loads to the switch actually alter the physical temperatures in the electronics box in a way that is not adequately monitored by the single thermocouple that outputs t_D .

In any case, it may be expected that the use of a single set of constants C_2 and C_4 evaluated with cold load 1 in the recommended data reduction process will lead to small uncertainties in the value of T_{SA} when cold load 2 is used for calibration. These uncertainties would be less than $1/2^\circ\text{K}$, for example, if the preflight calibration values of C_2 and C_4 were used.

The final type of uncertainty considered here arises from the fact that the "single-pass" procedure adopted for processing the data at JSC (See PHO-TR524.)* uses only the calibration immediately preceding a given data point. Because most data points are bracketed by a prepass and a postpass calibration, only half the available calibration data are used. Because of the magnification of the quantization error produced by the factor $(A_H - A_C)^{-1}$, a half bit error in A_H and A_C can produce uncertainties on the order of 1°K in T_{AC} at sea temperatures, on the order of 2.5°K at deep space temperature, and negligible at 300°K . In addition, the drift of t_D , T_{SC} , and T_{SH} from their prepass calibration values is largest just before the postpass calibration. The combined effect of these uncertainties may be estimated from analysis of T_{SA} from the passes on DOY 150, DOY 215, and DOY 216 referred to in paragraph II.B.

*Earth Resources Processing Requirements for EREP Electronic Sensors, PHO-TR524, Lyndon B. Johnson Space Center, Houston, Texas, January 3, 1974.

where 1 to 3°K discrepancies were noted between the use of prepass and postpass calibrations. Thus, the electronics box or receiver noise temperature appear to depend on cold-load temperatures, probably due to inadequate cable transfer relationships or incomplete measures of the electronics-box physical temperatures. The uncertainty of the receiver noise adds to the uncertainty in the final antenna brightness-temperature determination.

This Appendix contains a few of the applicable analysis techniques employed in the S194 Sensor Performance Evaluation Tasks by the contributors to this document (See Section 7.1). Additional analysis techniques and further details are contained in MSC-05528.